Development and operating experience of a 1.1-m-long superconducting undulator at the Advanced Photon Source

Y. Ivanyushenkov, K. Harkay, M. Borland, R. Dejus, J. Dooling, C. Doose, L. Emery, J. Fuerst, J. Gagliano, Q. Hasse, M. Kasa, P. Kenesei, V. Sajaev, K. Schroeder, N. Sereno, S. Shastri, Y. Shiroyanagi, D. Skiadopoulos, M. Smith, X. Sun, E. Trakhtenberg, A. Xiao, A. Zholents, and E. Gluskin

Advanced Photon Source, Argonne National Laboratory, 9700 South Cass Avenue, Argonne, Illinois 60439, USA

(Received 11 November 2016; revised manuscript received 18 July 2017; published 3 October 2017)

Development of superconducting undulators continues at the Advanced Photon Source (APS). Two years after successful installation and commissioning of the first relatively short superconducting undulator "SCU0" in Sector 6 of the APS storage ring, the second 1.1-m-long superconducting undulator "SCU1" was installed in Sector 1 of the APS. The device has been in user operation since its commissioning in May 2015. This paper describes the magnetic and cryogenic design of the SCU1 together with the results of stand-alone cold tests. The SCU1's magnetic and cryogenic performance as well as its operating experience in the APS storage ring are also presented.

DOI: 10.1103/PhysRevAccelBeams.20.100701

I. INTRODUCTION

Magnetic simulations suggest that superconducting undulators (SCUs) outperform other undulator technologies in terms of undulator peak field B for a given period length and magnetic gap [1–3]. As a result, superconducting undulators have the potential to significantly boost the brightness of high-energy x-ray beams, and therefore attracting the interest of the light source community in developing this technology [4–10].

The expected performance of superconducting undulator technology has been confirmed at the APS by the measurements of the photon flux of the first test superconducting undulator—SCU0. This undulator with a 0.3-m-long magnet generates higher photon flux than a 2.4-m-long hybrid undulator at photon energies above 80 keV [11], albeit in a narrower range of energies.

The experience of operating SCU0 demonstrates that the beam heat load has been correctly estimated taking heat leaks into account, a cryocooler-based cooling system has proved to be efficient, helium loss-free operation is possible, and cryocooler-induced mechanical vibrations do not disturb the beam. SCU0 was successfully operated in all bunch timing patterns at the APS without issues from beam-induced heating. At least for this short device, we showed that an SCU with sufficient field quality can be built without magnetic tuning. We also demonstrated that SCU quenches do not cause a beam dump and that the SCU beam chamber does not require baking.

The next logical step was to increase the length of the SCU magnet. Such a milestone was achieved with SCU1—the second superconducting undulator developed at the Advanced Photon Source (APS), as seen in Fig. 1.

In this paper we first give a concise description of the SCU1, with an emphasis on magnetic design and expected heat loads. We then describe the results of a stand-alone cooldown test, including magnetic measurements and cryogenic behavior of the SCU1. Finally, we present our experience of operating the SCU1 in the APS storage ring by describing the observed heat loads in the SCU1, the undulator performance, and its effect on the electron beam.

II. DESIGN OF SCU1

Superconducting undulator SCU1 was installed in Sector 1 of the APS storage ring. The parameters of SCU1 are listed in Table I. The period length of 18 mm was chosen to have continuous photon energy coverage above 40 keV. The length of the magnet is 1.1 m—more than 3 times the magnetic length of the SCU0.

Below we present the main conceptual points of the SCU1 design. A more detailed description can be found in [12–14].

A. Magnetic design

The SCU1 magnet is continuously wound with a NbTi superconducting wire onto a low-carbon steel former or core. The shape of the SCU1 core is similar to the SCU0 core shown in Fig. 2, but the mechanical design and conductor winding scheme were modified based on the experience of fabrication of the SCU0 cores.

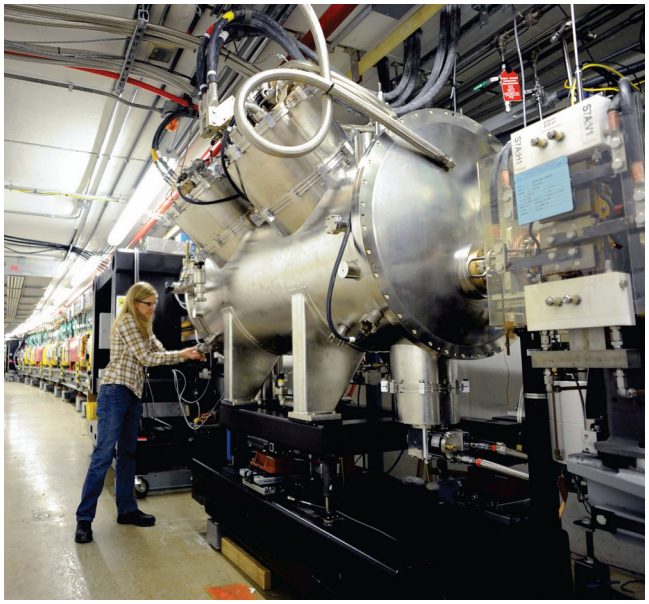

FIG. 1. Superconducting undulator SCU1 in the APS storage ring.

In the modified design, the magnetic poles are present only on the beam-facing side of the core, see Fig. 3. These poles are mechanically polished to guarantee an excellent surface finish and therefore prevent damaging conductor insulation during the winding process. The winding groove spacers on the other sides of the core are made of G10 material rather than steel. They are attached to the core body by spring pins. The winding scheme is also different from the one used in the SCU0 magnet. Instead of first winding all the odd grooves and then making a 180-degree turn and winding back all the even grooves, the conductor is turned around a pin on the back side of the core after winding each groove. In addition, the three liquid helium (LHe) channels in the SCU0 core are replaced with a larger diameter single channel in the SCU1 core. As a result of the design simplification, the cost of a 1.1-m SCU1 core is about the same as that of a 0.3-m-long SCU0 core. It is

TABLE I. Design parameters of SCU1.

Parameter	Value
Electron beam energy (GeV)	7
Photon energy at the fundamental (keV)	11.7–25
Period length (mm)	18
Number of periods	59.5
Vacuum gap (mm)	7.2
Magnetic gap (mm)	9.5
Design magnetic field (T)	0.97
Design operating current (A)	450
Design undulator parameter K	1.63
Magnetic length (m)	1.075
Cryostat length (m)	2.063

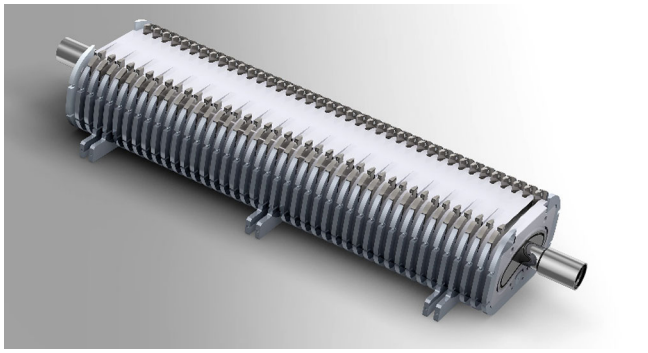

FIG. 2. SCU0 undulator magnet core.

worth highlighting that the SCU1 cores were fabricated to a very high precision, with measured groove dimensions, the period length, and the core planarity within 30 μm rms.

As in SCU0, a commercially available NbTi superconducting round wire was used in the SCU1 magnet, except that a wire diameter of 0.6 mm was chosen instead of the 0.7-mm diameter used in SCU0. The smaller wire size allows more turns, thus reducing the operating current of the magnet and therefore decreasing the heat leak through the current leads.

Several correction coils are available during operation of the SCU1. All of the correction coils are inside the cryostat. As a result of winding the undulator magnet with an odd number of main coil packs, there is a vertical field along the length of the undulator which is zero at the center of the magnet and increases linearly toward the ends. This field causes the electron trajectory to take an "S" shape. On each core there are correction coils wound in the two end grooves where there are a reduced number of turns of the main coil, see Fig. 4. These coils are referred to as end

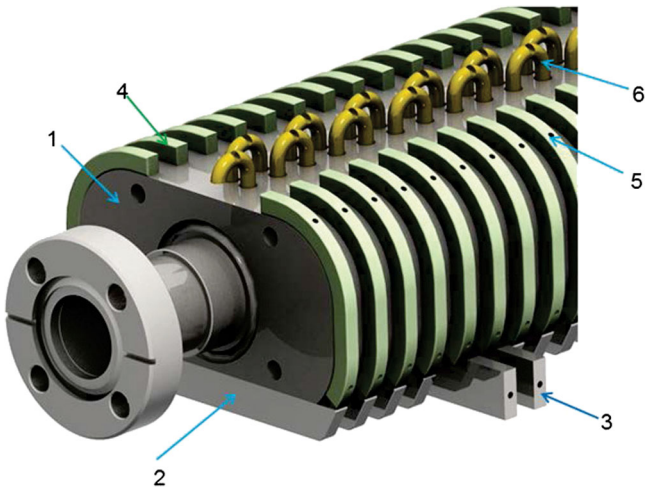

FIG. 3. SCU1 undulator upper magnet core. Core components: core body (1); magnetic poles (2); magnetic poles with the end tabs (3); G10 side spacers (4); spring pins (5); conductor turn around pins (6). The flanged pipe is for liquid helium cooling.

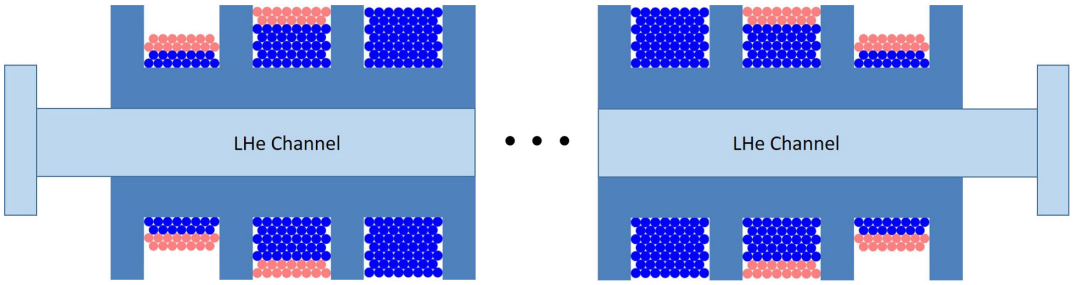

FIG. 4. Winding scheme of the SCU1 magnet. There are 53 conductors in a full main coil pack (blue), 38 main coil conductors in the second to last grooves, and 15 main coil conductors in the end grooves. There are 15 conductors (red) wound over the top of the main coil to form the corrector coil in the last two grooves at either end.

corrector coils and are wound with the same conductor as the main coil. The end corrector coils are used to straighten the electron trajectory as well as adjust the magnetic strength of the end poles. In order to correct the first field integral due to the measured undesirable dipole field (described in Sec. III B), there is a Helmholtz-like coil that is wound from ten turns of 0.7-mm diameter NbTi superconducting wire. These coils are placed above and below the assembled SCU magnet as shown in Fig. 5. The last type of correction coils available are used to adjust the second field integral. These are the dipole coils that are installed inside the cryostat upstream and downstream of the magnetic structure, as seen in Fig. 6. The coils are wound using 22 American wire gauge copper magnet wire.

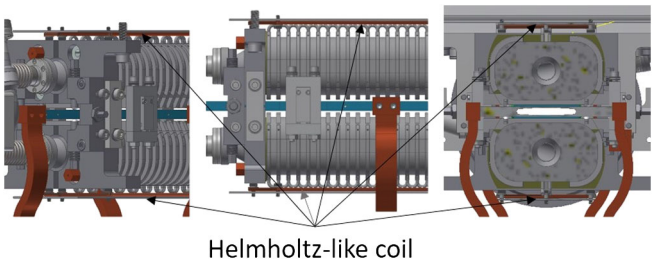

FIG. 5. Helmholtz-style coil to correct the dipole vertical field along the length of the device.

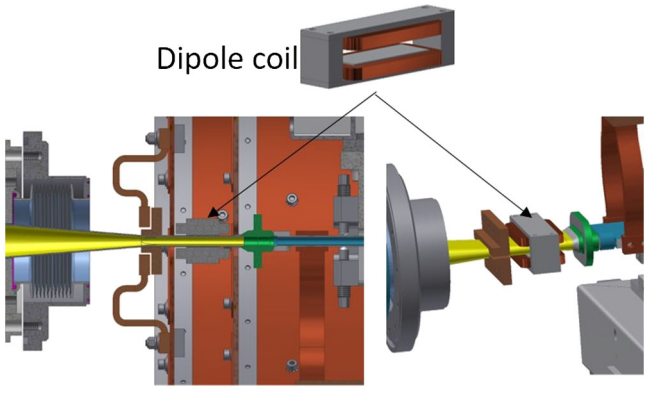

FIG. 6. Dipole coils installed upstream and downstream of the undulator magnet inside the cryostat that can be used to compensate the second field integral.

B. Cryostat

The SCU1 uses a cryostat that is an improved version of the SCU0 cryostat [13]. Modifications include the addition of optical windows in the cryostat vacuum vessel that allow direct observation and measurement of the cold mass vertical position inside the cryostat. Also, several thermal links were added to improve cooling of the cold mass support frame. The Kevlar strings that support the cold mass in the cryostat have been improved as well. We plan to devote a separate paper to a detailed description of several generations of SCU cryostats.

C. Predicted heat loads

As noted earlier, the analysis of anticipated heat loads on the superconducting magnet is crucial for the design of the superconducting undulator cooling circuit. The total heat load in the superconducting undulator includes both static heat loads, which are typical for superconducting magnets, and the heat load from the electron beam. The beam heat load includes heating of the SCU vacuum chamber by beam-induced image currents, synchrotron radiation generated in upstream dipole magnets, wakefield effects, particle losses, and, potentially, electron cloud-induced multipacting (the latter has not been observed at APS).

Under nominal operating conditions, cw (or equilibrium) heat loads are present from several of these effects, while specific machine fault conditions may occur that give rise to transient heat loads.

Because the beam-induced power is intercepted by the SCU vacuum chamber, and the SCU1 vacuum chamber is the same design as the SCU0 vacuum chamber, predictions of the various contributions to the cw heat load for SCU1 are the same as SCU0. Details of the beam-induced heat load calculations can be found in Ref. [11]. As in SCU0, the SCU1 chamber was polished to obtain surface roughness on the order of 0.1 μm rms. This limits the roughness-related increase in surface resistance and, therefore, increases the power deposited on the walls by only 10%

compared to a perfectly smooth surface. The SCU1 vacuum chamber warm transitions are the same as for SCU0, and were designed to minimize wakefield heating in the warm-to-cold transition tapers.

As in SCU0, a photon absorber is present that is intended to mask the SCU1 chamber walls from photons from the upstream dipole magnet. Analyses were performed for large electron beam orbit displacement and angle errors that could occur during a fault condition, such as a steering corrector error. The analysis assumes a single orbit distortion source limited by the physical chamber aperture, and does not take credit for the beam position limit detector system (BPLDs) [15]. The results show that the SCU1 chamber is passively shielded from dipole radiation for all possible horizontal trajectories in the dipole magnet. On the other hand, large vertical orbit displacements and/or angle errors can potentially cause a synchrotron radiation heat load of up to 25 W on the SCU1 chamber walls. Since the photon absorber does not shield the chamber from vertical orbit steering, the vertical electron beam steering is restricted administratively to ± 1 mm and ± 0.1 mrad at the dipole magnet. The resulting heat load is then limited to 5 W. In practice, the vertical beam steering at the dipole magnet is much smaller, with the resulting heat load limited to <1 W.

Based on these analyses, the maximum cw heat load on the vacuum chamber during normal operation was estimated to be less than 9.5 W at 20 K, the same as for SCU0. The design value for the heat load at the 20-K stage was increased to 14 W to include heat load by the corrector coils mounted on the beam vacuum chamber, as well as an additional heat load on the inner thermal shield that is also connected to this thermal stage. The SCU1 20-K stage cooling system has a capacity of 40 W, as listed in Table II, which provides a comfortable margin for normal operation.

Transient heat loads could potentially occur under various fault conditions that cause beam orbit displacement or angle errors; peak heating up to 25 W over a short time interval of $\lesssim 1$ sec is possible. Temperature monitoring using thermal sensors mounted on the chamber detects anomalous heating, and temperature interlocks shut off the SCU1 power supply to prevent the magnet from quenching. In practice, anomalous beam heating is not observed during user operations because the BPLD system is engaged and limits the beam orbit offset to about ± 0.5 mm vertically and ± 1 mm horizontally.

TABLE II. Design heat loads and installed cooling capacity.

Heat source	Temperature (K)	Design load (W)	Installed capacity (W)
Magnet	4.2	0.6	~1.5
Vacuum chamber and inner radiation shield	20	14	40
Outer radiation shield	60	87	224

III. COLD TEST RESULTS

A. Cryogenic test

The undulator was cooled down using four two-stage cryocoolers installed in the cryostat. Temperatures recorded during a typical 72-hour cooldown are shown in Fig. 7. Following cooldown, the internal tank is filled with 50 liters of LHe.

Electron beam heating was simulated by powering an electric heater connected to the cold part of the beam chamber. As expected, the temperature of the beam chamber did increase but the magnet temperature was stable, as listed in Table III. This test demonstrates excellent thermal isolation of the superconducting magnet from the beam chamber.

As in SCU0, the cooling power provided by the cryocoolers in the SCU1 exceeds the heat load on the 4-K circuit, thus providing excess cooling power at this thermal stage. To stabilize the pressure in the LHe circuit in this situation, heat is periodically applied to the LHe tank using a heater mounted on the tank surface. By measuring the duty cycle of this heater and knowing its power, one can calculate the excess cooling capacity at 4 K. The excess cooling capacity is about 400 mW for a static condition when the magnet is not powered, and is about 360 mW with the magnet powered to the design operating current of 450 A. When 20 W is applied to the beam chamber, the excess cooling power reduces to about 280 mW. It should be noted that in SCU0, which has a similar beam chamber, the measured electron beam heat load on the beam chamber is about 15 W with a beam current of 100 mA in 24 bunches with the user operation beam orbit. This represents reasonably good agreement with the predicted beam heat load. It is difficult to compare the SCU1 heat load analysis with cryogenic devices elsewhere, given the markedly different geometry and vacuum elements. However, others have recently achieved similar agreement when detailed studies were carried out [16].

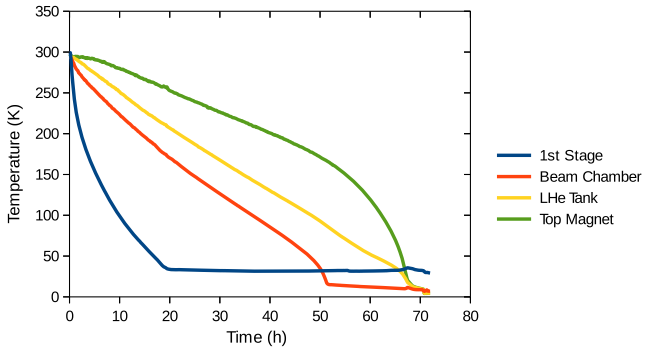

FIG. 7. Temperatures of the SCU1 components during the cooldown process: the 1st stage of 4-K cryocooler (blue); beam chamber (red); LHe tank (yellow), and the magnet top core (green).

TABLE III. Observed temperatures of the beam chamber and the magnet during beam heat load simulation test.

Magnet current (A)	Heater power (W)	Beam chamber temperature (K)	Magnet temperature (K)
0	0	7.26	4.22
450	0	7.26	4.22
450	20	14	4.22

B. Magnetic measurements

Before installation in the cryostat, the SCU1 magnet was assembled and tested in a vertical liquid helium bath cryostat. The goal of this test was to train the magnet and to make preliminary measurements of the magnetic field profile with a Hall probe. The quench currents during training are shown in Fig. 8. The training process was completed within four days. It is evident from the data that it required about 70 quenches to train one core and about 140 quenches for training the other core. Longer training of the second core might be related to the imperfect quality of the core epoxy resin impregnation because of a deviation from an impregnation procedure. For comparison, the approximately 3-times shorter SCU0 cores required 21 training quenches for one core and 26 for the other. One can therefore suggest that the number of training quenches seems to scale linearly with the number of coil packs in the core, and roughly linearly with the length of the SCU magnet core. This is a very preliminary conclusion, the correctness of which will be checked when more superconducting undulator magnets are built and trained.

It should be noted that after installation into the horizontal cryostat, the magnet reached the operation current after only ten quenches.

Initial magnetic measurements with a Hall probe in the LHe bath cryostat indicated that an unexpected vertical dipole component at a level of a few mT existed in the undulator field. To compensate for this undesirable field, a Helmholtz-like dipole corrector was added to the magnetic structure. The results of the magnetic measurement shown below were taken with this corrector switched on.

We are currently running magnetic simulations to search for a source of the observed dipole field. The magnetic model in RADIA [17] includes two magnet cores separated by a magnetic gap. Each core consists of a set of winding packs, magnetic poles and a magnetic core body with a LHe channel in it. Preliminary modeling indicates that a vertical dipole field might be caused by a horizontal displacement of the LHe channel in one of the magnetic cores although this has not yet been proved experimentally. A more rigorous analysis is being continued in both RADIA and OPERA [18].

Once the assembly of the SCU1 in the cryostat was completed, the magnetic performance of the undulator was measured with the magnetic measurement system previously developed and used for the measurements of SCU0 [19]. The magnet excitation curve is shown in Fig. 9. At the design current of 450 A the undulator delivers the expected field of 0.976 T. The quench current is about 520 A, thus giving a comfortable margin for device operation.

As with SCU0, the undulator's vertical magnetic field was measured with a moving Hall probe. A typical field profile is shown in Fig. 10. The analysis of the measured field at the maxima and minima gives the average peak field value of 0.96745 T with a standard deviation of 0.00469 T. The half period length is calculated as 8.976 mm with a standard deviation of 0.012 mm. The phase errors shown in Fig. 11 were calculated from the Hall probe measurements after disregarding five poles from each end of the undulator. At the design current of 450 A, the measured phase error is about 5.3° rms. It is worth mentioning that analysis of the field profile showed that substantial contributions to the total value of the phase errors came from five periods at both ends of the device. The magnetic gaps at the ends were larger by about 300 μm due to bowing of the magnetic cores during vacuum resin impregnation, contributing to the gap profile inhomogeneity. A special gap correction system based on a set of mechanical clamps will be implemented in our next undulator.

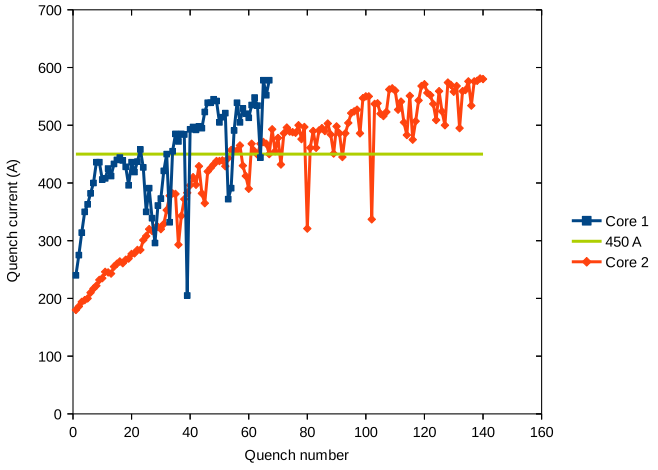

FIG. 8. Quench currents during training of cores.

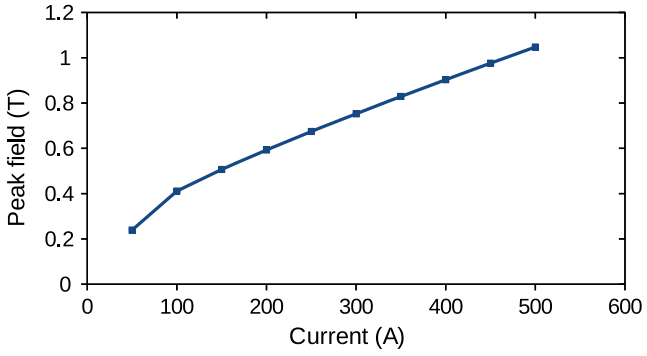

FIG. 9. Magnet excitation curve.

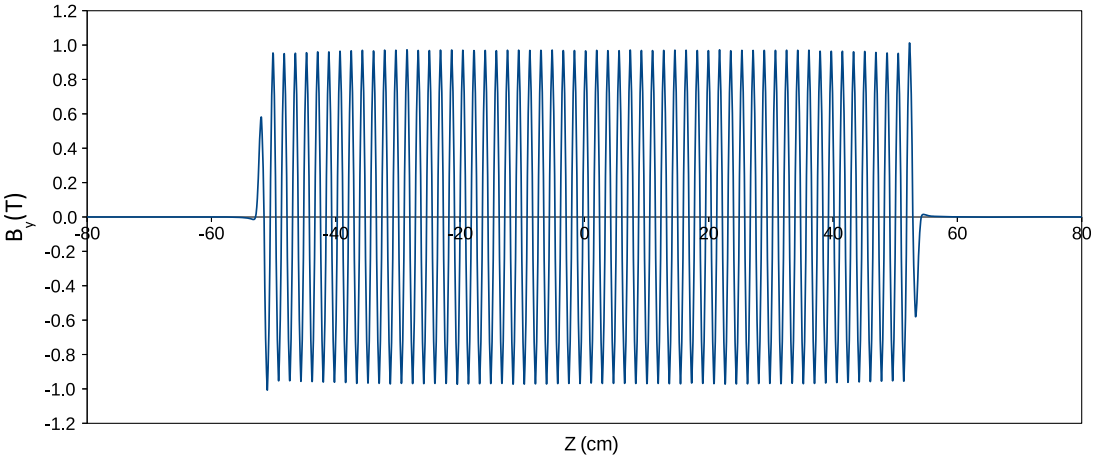

FIG. 10. Measured undulator field profile at magnet current of 450 A.

The first and second field integrals were measured on axis with stretched wire coils. The first field integrals varied between -25 and -40 μT m for magnet currents in the range of 50–500 A, while the second field integrals varied between 120 and 420 μT m^2. The measured first field integral is well within the specification of $|I_{1y}| < 80$ μT m while the second integral exceeds the requirement of $|I_{2y}| < 102$ μT m^2. This issue and how we dealt with it is discussed in more detail in Sec. IV C 2.

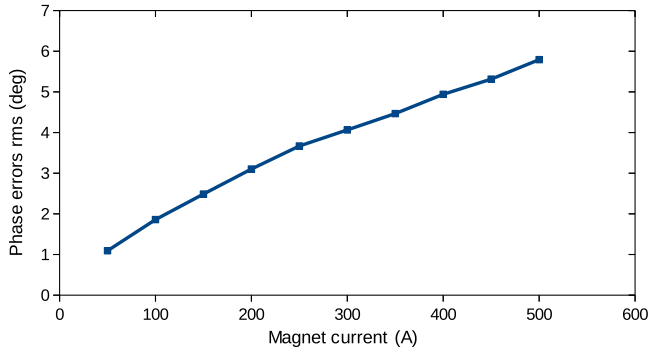

FIG. 11. Measured phase errors as a function of magnet current.

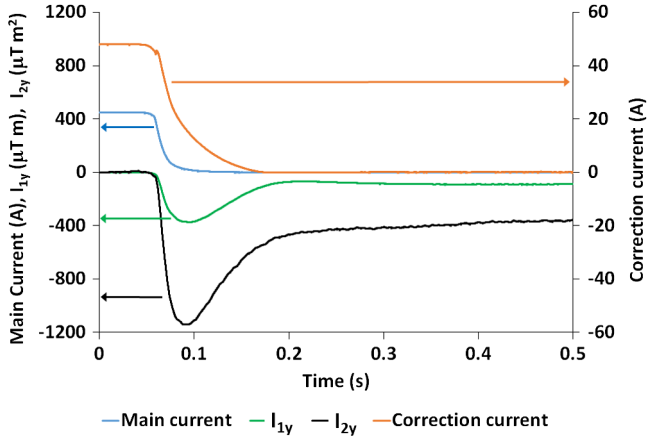

FIG. 12. Measured first and second field integrals during quench test.

Dynamic behavior of the field integrals was measured during quenches triggered by heaters mounted on the magnet cores. The first and second vertical field integrals I_{1y} and I_{2y} are shown together with the main coil and end corrector coil currents during such a quench in Fig. 12. The measured dynamic variation of the field integrals are sufficiently small as to not cause an electron beam trajectory deviation that exceeds the beam position limit detector limits, which would in turn trigger a beam dump.

IV. SCU1 OPERATING EXPERIENCE

A. Commissioning

In order to ensure continued reliable operation of the facility for APS users, stringent requirements must be met by all insertion devices that are installed in the APS storage ring. For SCU1, these requirements were: (a) When unpowered, SCU1 is transparent to normal user operation; i.e., it does not measurably increase the storage ring impedance, or decrease the injection efficiency or electron beam lifetime. (b) When powered, SCU1 only perturbs the beam within the beam stability specifications; and (c) SCU1 is sufficiently protected from beam-induced heat loads, i.e., does not exceed the cryosystem cooling capacity (Table II). The detailed SCU0 commissioning plan was revised, given the experience commissioning that device, compressing the overall commissioning time for SCU1 by a factor of 3. The following commissioning steps were included: assessment of magnet alignment, cryogenic performance, beam orbit stability, quench response, end-coil field correction, and x-ray performance. Approximately 30 hours were used for SCU1 commissioning, with about half of the time used to tune the end-coil field correction.

TABLE IV. APS SCU operational statistics.

		SCU0			SCU1		
Calendar year	APS delivered h	Operating h	Down h	Available %	Operating h	Down h	Available %
2013	4871	4189	20	99.6			
2014	4926	4391	174	96.5			
2015	4940	4834	0	100			
May–Dec, 2015	3241				3059	0.1	99.997
Jan–Aug, 2016	3402	3310	0	100	3226	0.3	99.991

B. Observed SCU1 behavior

1. Operational reliability

Table IV gives a summary of the SCU1 operational statistics. SCU0 statistics are also shown for comparison. Operating hours accumulate when the main coil current is above 50 A, and down hours accumulate when the device cannot be operated, in each case while user beam is delivered. Downtime typically occurs when the LHe cooling tank pressure is above a specified operating limit, such as after a quench. Availability is computed as [1-(SCU down h)/(APS delivered h)], and usage is computed as (SCU operating h)/(APS delivered h). SCU1 exhibited high availability (>99.99%) and usage (94.6%) starting in the first year of operation, a reflection of both its reliability and performance. The SCU0 lost some of LHe in November 2014, which contributed 149 h of downtime, but has since operated with no downtime. Over three years, SCU0 availability increased from 96.5% to 100%, and usage from 86% to 97%. The SCUs have self-quenched only a few times over many thousands of operating hours—once for SCU1 and six times for SCU0—and these quenches have not caused any beam trips. A few of the self-quenches occurred while the device current was ramping, and at least one occurred while the electron beam was being steered for another beam line. Given the low statistics and varying conditions, the precise cause of the self-quenches is not understood. Additional details on the effect of quenches on the beam are given in Sec. IV C 3.

2. Cooling system

Four cryocoolers provide the cooling power for SCU1. Table V shows that the actual temperatures in the system are at or below the design levels given in Table II.

TABLE V. SCU1 design and observed temperatures.

Parameter	Design temperature (K)	Observed temperature (K)
Superconducting magnet	4.2	4.25
Vacuum chamber	20	8–13
Internal thermal shield	20	8–11
Outer thermal shield	60	32–34

In the presence of the electron beam, the cooling system LHe pressure is stable and insensitive to the magnet current, as seen in the first week of user operations (Fig. 13.) This is a further indication that the cryocoolers provide adequate cooling, and that the magnets are isolated from beam-induced heating during normal operations.

After a quench, the energy stored in the coils is dissipated in the LHe, which raises the tank pressure. SCU1 is 3 times longer than SCU0 and, therefore, has 3 times more energy stored in the coils. However, recovery after a quench in SCU1 is nearly the same in duration as for SCU0. Figure 14 shows a beam-dump-induced quench of both devices, with an associated rise in the LHe tank pressure. The beam dump (unrelated to the SCUs) occurs just after "31d8h" (08:00 on May 31) on the plot. The SCU1 pressure (black) rises from a base pressure of 760 Torr to almost 900 Torr, while the SCU0 pressure (red) rises to about 820 Torr. The first fill after the quench is 24 bunches (from about 8:30 to 10:20), and the second fill is 324 bunches (from about 10:20 to 13:40). The cooldown rate is initially faster for SCU0 than for SCU1, but SCU0 cooldown significantly slowed down after the beam is restored, especially for the 24-bunch pattern. The SCU1 cooldown rate is far less affected by the beam because the thermal isolation of the beam vacuum chamber is improved compared to SCU0. Both devices may be operated after the LHe pressure reaches 830 Torr. As one can see in the figure,

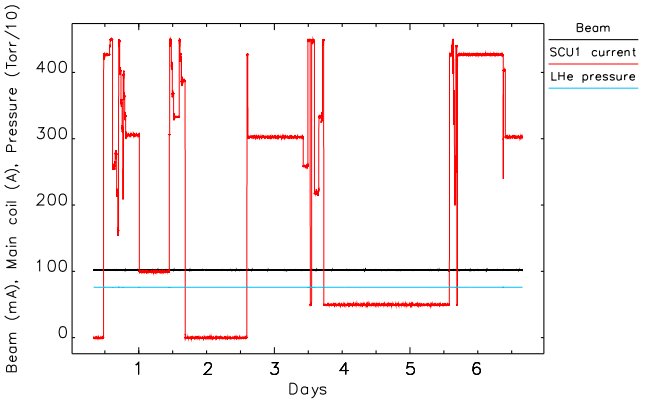

FIG. 13. First week of SCU1 operation. The ring was in top-up mode at 100 mA.

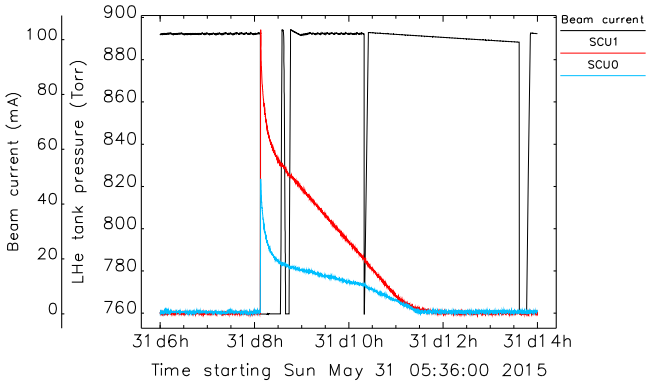

FIG. 14. Comparison of SCU recovery after a beam-dump-induced quench, as measured by the LHe tank pressure. Prior to the quench, the average magnet temperature was 4.23 K for SCU1 and 4.34 K for SCU0, and the main coil current was 450 A for SCU1 and 668 A for SCU0.

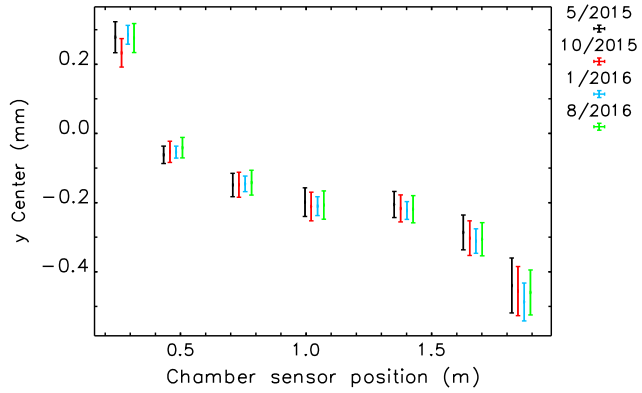

FIG. 15. Measured vertical position of the vacuum chamber inside the cryostat over a one-year period using the beam-based method.

SCU1 reaches the return pressure after about 30 min. After a quench, the magnet temperatures recover on a shorter time scale (i.e., a few minutes), as discussed below. The average beam recovery time is 20–30 min.

3. SCU1 magnet position stability

The vertical position of the SCU1 vacuum chamber, which is a part of the cold mass, was measured with the electron beam using a method developed at APS [20], applied also to SCU0. The electron beam is steered vertically within the chamber while observing the response of thermal sensors mounted on the chamber. The thermal sensor minima determine the vertical center of the SCU1 chamber with respect to the user orbit. The initial measurement in May 2015 showed an overall vertical chamber alignment at the SCU1 magnet cores (i.e., at the center five sensors) to be about -0.2 ± 0.15 mm relative to the user beam orbit. No realignment was required. SCU chamber alignment poses a unique challenge, given the extreme temperature changes in combination with limited access to the magnet structure and vacuum chamber [21]. The addition of the optical windows on the cryostat enabled greater precision in the initial chamber alignment compared to SCU0.

Similar alignment measurements were repeated several times over a year of operation. These demonstrate that the vacuum chamber position has remained stable since installation, as shown in Fig. 15. Thanks to the improvements made to the Kevlar support of the SCU1 cold mass, no slow shift has been observed in the position, unlike the case in SCU0.

4. Quenches

The SCU1 was found to quench during beam dumps triggered by the machine protection system (MPS), although far less frequently than SCU0 (both SCUs are powered off during intentional beam dumps.) A quench causes a magnet temperature rise from 4.25 K up to 10–14 K and a LHe pressure rise of about 140 Torr. It takes about 1–3 min for the core temperature to return to within 0.1 K of the prequench temperature (see the left panel in Fig. 16). The SCU0 core temperatures before and after a quench are also shown in the figure for comparison.

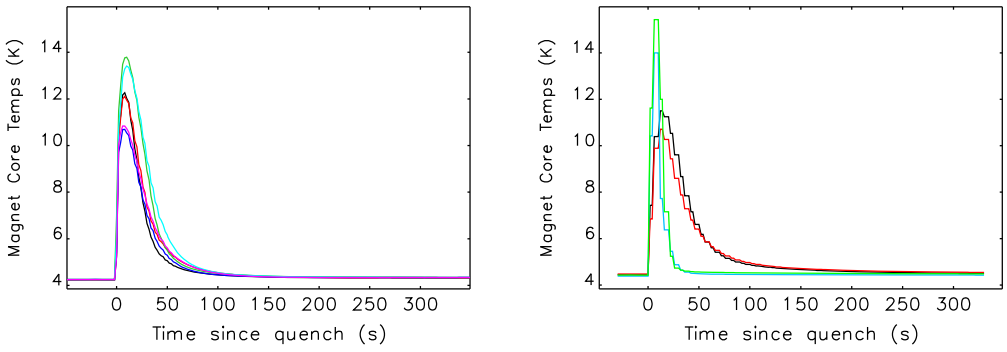

FIG. 16. Magnet core temperatures before and after a quench, measured by six (SCU1, left) and four (SCU0, right) temperature sensors on two magnet cores, shown in different colors. Prior to the quench, the main coil currents were 426 A for SCU1 and 666 A for SCU0.

Protection against beam-loss-induced quenches is a well-known issue in high-energy proton accelerators, where superconducting magnets have been used for several decades [22]. Machine protection interlocks typically include beam loss monitoring and beam abort systems. For almost as long, but mostly in the past 10–12 years, superconducting magnets—SCUs [10,11], wigglers [23], and superbends [24]—have been employed for the generation of high-energy photons in electron synchrotron light sources. While all superconducting wigglers and SCUs have quench-detection interlocks to protect the magnet, very little has been written about characterizing and preventing beam-loss induced quenches. A notable exception is at the Canadian Light Source, where the injection kickers were employed to also serve as an abort system to prevent such quenches [25].

At APS, simulations suggest that a beam loss of >50 pC deposits energy sufficient to raise the coil temperature above the critical temperature. This is a small fraction of the 375-nC (102 mA) circulating beam. To better control the beam loss location at the level required to prevent a quench, an abort kicker system was installed [26,27]. A dedicated, horizontal abort kicker is triggered by MPS and causes the beam to be lost at a location distant from the SCUs, within a few turns. In the eight months after installing the abort system, the SCU0 quench rate decreased dramatically from 80% to 14% of beam dumps, while the SCU1 quench rate remained approximately the same, from 23% to 19% of beam dumps. The abort system is estimated to be effective approximately 90% of the time; it is ineffective for approximately 10% of beam dumps where beam losses occur on the chamber walls before MPS detects beam centroid motion. We are planning to study beam-loss-induced quenches in more detail and to publish the results separately.

C. SCU1 effect on the electron beam

1. SCU1 transparency

Because the SCU1 beam vacuum chamber is virtually identical to SCU0, besides chamber alignment, no other effects on the beam were expected or observed. Like SCU0, there were no beam chamber vacuum pressure issues and no negative effects observed on the beam. Vacuum conditioning was similar. Mechanical vibration of the vacuum chamber caused by the SCU1 cryocoolers is expected to be similar to SCU0, given that the SCU1 cryocoolers are the same as SCU0 [11]. The vibration was not measured in SCU1, since nothing significant was seen for SCU0.

2. Magnetic performance

The first- and second-field integral perturbations (I_1 and I_2, respectively) for the vertical and horizontal fields of the device were measured on the bench, i.e. during a stand-alone cold test described in Sec. III B. B_y-field corrector coils are provided to compensate these perturbations, with their setting determined by magnetic measurements. Figure 17 shows the residual B_y field integrals of SCU1 with these initial settings, as measured by both magnetic measurement lab and the stored beam orbit after installation. The resulting perturbation on the stored beam satisfies the physics specification of $|I_{1y}| < 80\ \mu\mathrm{T\,m}$ but misses that of $|I_{2y}| < 102\ \mu\mathrm{T\,m^2}$ by a factor of ∼3.

To further prepare the SCU1 for operations, we adjusted its corrector coils a second (and final) time to reduce its perturbation as much as possible using the stored beam orbit itself as a guide. The peak of the resulting $|I_{2y}|$ is about 200 $\mu\mathrm{T\,m^2}$ during a ramping cycle from 0 to 450 A and back to 0 A, mostly due to the hysteresis observed between 0 and 100 A. Because the feedforward correction table applies values irrespective of ramp direction, we cannot make separate corrections for both ramp directions.

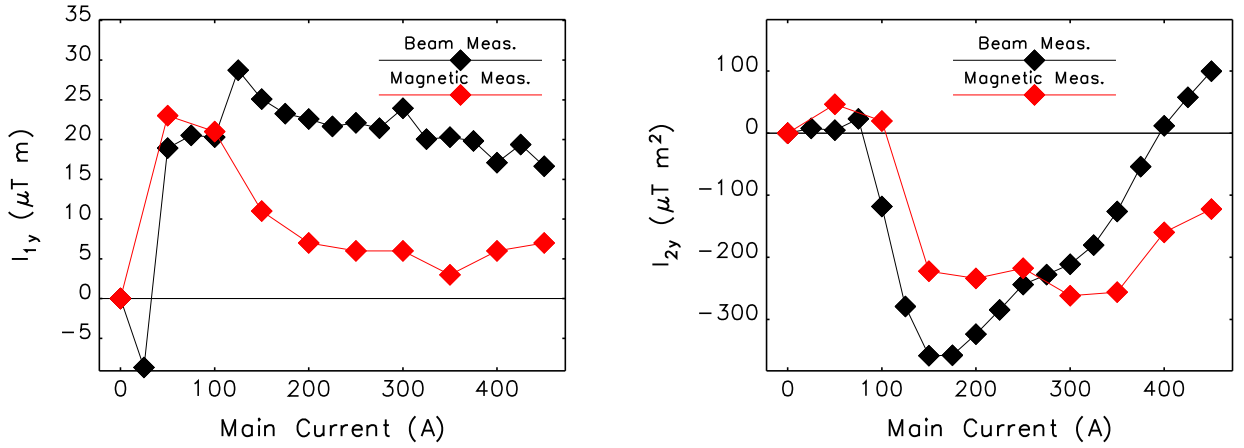

FIG. 17. Vertical-field integrals of initial correction as measured using the stored beam, before final beam-based adjustments. The first integral is on the left and the second integral is on the right.

On the other hand, the useful range of operation of SCU1 is between 100 and 450 A, outside of the problematic hysteresis range. The variation of I_{2y} in this operating range is $\pm 50\,\mu\mathrm{T\,m^2}$ (compare this to the original I_{2y} in Fig. 17), so that the device satisfies the requirements most of the time.

There are no corrector coils for the horizontal fields, since the measured perturbation (in the lab) was smaller than the physics specifications of $|I_{1x}| < 25\ \mu\mathrm{T\,m}$ and $|I_{2x}| < 32\ \mu\mathrm{T\,m^2}$.

The only multipole components that could be easily measured with beam are the quadrupole normal and rotated components, whose effect on the beam are tune shift and x- and y-emittance ratio, respectively. If there are any effects, they are below the threshold of measurement. The lifetime of the beam is unchanged when the SCU1 is operating at full current, indicating that higher-order multipoles effects, if any, are negligible.

3. Effect of quenches

Quenches may produce a field disturbance on a time scale that is too fast for the fast orbit feedback [28] to correct. If the perturbation is very large, the resulting beam trajectory displacement at the undulators could exceed the BPLD limits and cause a beam dump. The maximum orbit perturbation is proportional to the quantity $\mathcal{A} = \sqrt{I_1^2 + (I_2/\beta_\mathrm{U})^2}$, where I_1 and I_2 are the changes in the first and second field integrals, respectively, and β_U is the average beta function at the undulator ends. To avoid dumping the beam during a quench, using a maximum horizontal displacement of ± 1 mm, the specification for $\mathcal{A}$ for the B_y fields is $720\ \mu\mathrm{T\,m}$. With a peak $\mathcal{A}$ value of $377\ \mu\mathrm{T\,m}$ for the B_y fields measured during an induced quench (see Fig. 12), SCU1 meets the field quality specifications. The B_x fields are negligible.

Tests with the beam, shown in Fig. 18, demonstrate that a heater-induced quench produced maximum horizontal beam motion of about ± 0.6 mm without fast orbit feedback running. Fast orbit feedback reduces the orbit perturbation by a factor of 5, bringing it well within the BPLD trip level and, as a result, a quench does not cause loss of the beam. As seen in Fig. 18, slow orbit recovery occurs over about 1 sec. There was no detectable vertical beam orbit motion.

Besides MPS-dump-induced quenches, during normal APS stored-beam operations SCU1 self-quenched only once over its first year of operation. This quench did not cause any beam loss, and quench recovery did not affect storage ring operations. The impact of all quenches on SCU1 operation, including those that occur on occasion with MPS-triggered beam dumps, has been minimal due to rapid SCU1 recovery, typically less than 30 min.

D. Photon flux measurements

The SCU1 device was intended to meet scientific program requirements of the APS 1-ID high-energy x-ray beam line, operating over the 40–140 keV energy range with full tunability. Prior to the installation of SCU1, beam line 1-ID had two hybrid-permanent-magnet, planar insertion devices U33 and U23, with 3.3 and 2.3 cm periods, respectively (the former also known as an APS Undulator A). Having 2.4 m magnetic lengths each, together they occupied the 5 m straight section. Due to thermal load limits on the beam line's x-ray front end, only one of these two devices was used at a time, subject to an 11.0-mm minimum magnetic gap. U23 delivered typical undulator radiation having a characteristic central cone, dominated by the electron emittance. U33, originally designed to provide undulator radiation properties at lower energies, delivered high flux at high energies when operating near minimum gap, but with larger beams corresponding to wigglerlike radiation with low-K. Due to the suitability of U33's larger, high-flux beams for certain experiments, SCU1 was installed in replacement of U23 in May 2015, with U33 remaining in place.

Figure 19 shows the flux comparison among U33, U23, and SCU1 sources, measured with monochromatized radiation over 40–140 keV at 1-ID, under the same beam line conditions. The flux measurements were made with a N_2-gas-filled ionization chamber placed after the beam

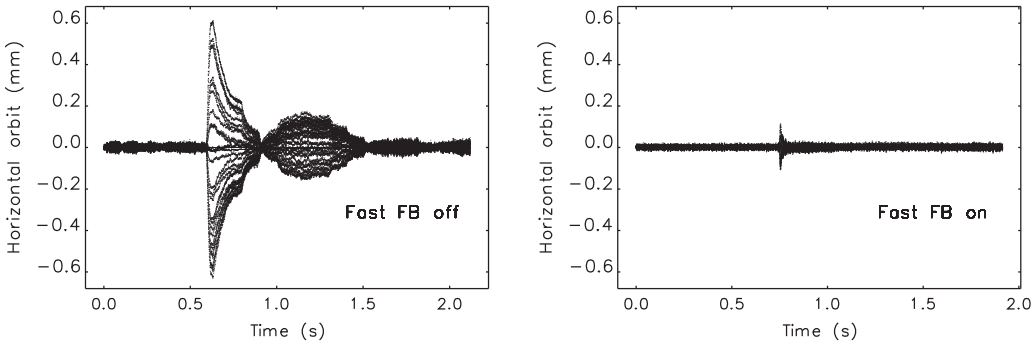

FIG. 18. Effect of induced quench on the beam orbits at all the insertion devices (IDs). Left panel: Slow orbit correction only. Right panel: Fast orbit feedback (FB) turned on.

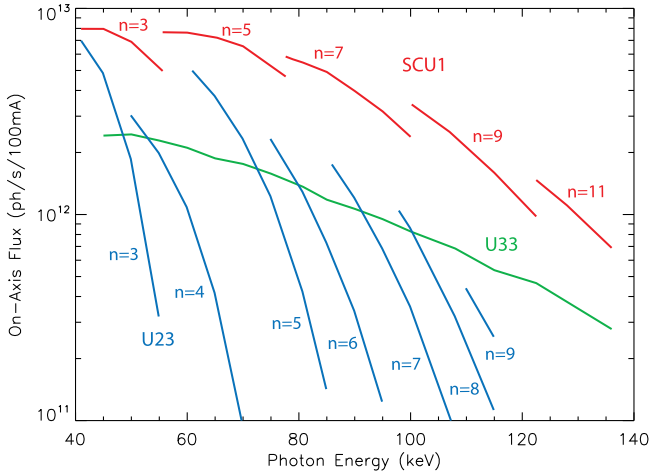

FIG. 19. Measured odd-harmonic SCU1 tuning curves (450 A maximum) of monochromatic flux through a 0.5×0.5 mm^2 aperture at 27.5 m compared with those of 11-mm minimum-gap permanent magnet devices U33 (continuous tuning curve envelope) and U23 (even and odd harmonics).

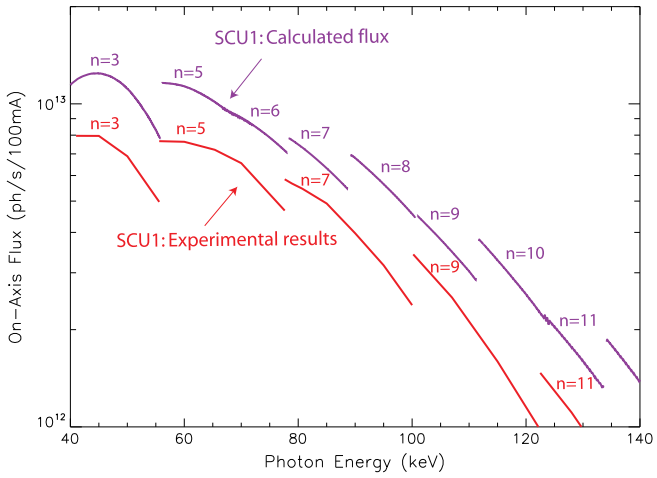

FIG. 20. Comparison of measured and expected SCU1 flux.

line's bent double-Laue monochromator [29]. The white beam was apertured to 0.5×0.5 mm^2 at 27.5 m from the source. In propagation, the beam experienced attenuation from Be windows (1.27 mm), graphite filters (2.0 mm), Al (0.017 mm), and air (1.55 m), in addition to transmission through the Si monochromator crystals (5.0 mm total). Over 40–140 keV, the monochromator's integrated bandwidth $\Delta\lambda/\lambda$ increases through the range 0.03%–0.14%. The measurements show SCU1's considerable gains over the other two permanent magnet undulators, with the largest gain being a factor of ~4 near 60, 80, and 100 keV where the SCU1 5th, 7th, and 9th harmonic tuning curves begin. The odd harmonics 3, 5, 7, 9, 11 of SCU1 give full spectral coverage over the operational energy range of 1-ID with enhanced flux and brilliance, advancing all of the beam line's programs. Due to its electromagnetic nature, with a mechanically fixed magnetic gap, SCU1 exhibits extremely high stability and reproducibility of spectral peaks as a function of undulator magnet current, which has proved to be very convenient from the beam line operations standpoint.

Figure 20 again shows the measured SCU1 flux, compared to a calculation of the expected flux that accounts for the measured magnetic fields, monochromator bandwidth, and beam line attenuators. The flux calculations were obtained with the computer code SPECTRA [30], using measured magnetic fields as input. The measured flux is ~2/3 of the calculated flux, which is reasonable given the nontrivial nature of absolute flux determination. This included uncertainties in modeling of the ionization chamber response (used to convert the raw signal to photons/second) and the bent-crystal monochromator performance at high energies (used to correct the calculated flux).

V. SUMMARY

A second planar superconducting undulator, SCU1, has been installed in the APS storage ring and successfully operated since spring of 2015. SCU1 cryogenic performance is well understood and was characterized in detail to improve the next generation of SCU insertion devices (IDs). Detailed beam studies with SCU1 confirmed the predicted behavior of the undulator and did not reveal any surprises in the beam induced heat loads or in the beam dynamics. A newly installed beam-abort kicker significantly improved SCU1 protection from beam-dump-induced quenches. Over its operating range, SCU1 magnetic performance meets APS ID specifications and there is a clear path for the improvement of newly built SCUs. SCU1—a 1.8-cm period, 1.1-m-long ID—significantly outperformed an optimized 2.4-m-long hybrid permanent magnet ID in the high energy part of x-ray spectrum. It is a highly reliable device with the availability close to 100%. APS will continue to design and build new SCUs for the next generation of storage rings and FELs.

ACKNOWLEDGMENTS

The authors acknowledge the long-term continuous support of the APS management. We also thank the APS staff for many valuable contributions. This work is supported by the U.S. Department of Energy, Office of Science, under Contract No. DE-ACO2-O6CH11357.

[1] P. Elleaume, J. Chavanne and B. Faatz, Design considerations for a 1 Å SASE undulator, Nucl. Instrum. Methods Phys. Res., Sect. A **455**, 503 (2000).

[2] E. Wallén, J. Chavanne, and P. Elleaume, Status of the development of superconducting undulators at the ESRF, in *Proceedings of the 9th European Particle Accelerator*

Conference, Lucerne, 2004 (EPS-AG, Lucerne, 2004), pp. 378–380.

[3] J. Bahrdt and Y. Ivanyushenkov, Short period undulators for storage rings and free electron lasers, J. Phys. Conf. Ser. **425**, 032001 (2013).

[4] C. S. Hwang, J. C. Jan, P. H. Lin, C. H. Chang, M. H. Huang, F. Y. Lin, T. C. Fan, and H. H. Chen, Mini-pole superconducting undulator for x-ray synchrotron light source, IEEE Trans. Appl. Supercond. **16**, 1855 (2006).

[5] S. Casalbuoni, M. Hagelstein, B. Kostka, R. Rossmanith, M. Weisser, E. Steffens, A. Bernhard, D. Wollmann, and T. Baumbach, Generation of x-ray radiation in a storage ring by a superconductive cold-bore in-vacuum undulator, Phys. Rev. ST Accel. Beams **9**, 010702 (2006).

[6] J. C. Jan, C. S. Hwang, P. H. Lin, and F. Y. Lin, Design and improvement of a mini-pole superconducting undulator at NSRRC, IEEE Trans. Appl. Supercond. **18**, 427 (2008).

[7] C. S. Hwang, J. C. Jan, C. S. Chang, S. D. Chen, C. H. Chang, and T. M. Uen, Development trends for insertion devices of future synchrotron light sources, Phys. Rev. ST Accel. Beams **14**, 044801 (2011).

[8] Z. Zhang, J. Xu, J. Cui, W. Li, M. Li, J. Xu, J. Yu, and Y. Jiang, Design of a superconducting undulator magnet prototype for SSRF, in *Proceedings of the 4th International Particle Accelerator Conference, IPAC-2013, Shanghai, China, 2013* (JACoW, Shanghai, China, 2013), p. 2013.

[9] P. Emma, N. Holtkamp, D.-H. Nuhn, D. Arbelaez, J. Corlett, S. Myers, S. Prestemon, R. Schlueter, C. Doose, J. Fuerst, Q. Hasse, Y. Ivanyushenkov, M. Kasa, G. Pile, E. Trakhtenberg, and E. Gluskin, A plan for the development of superconducting undulator prototypes for LCLS-II and future FELs, in *Proceedings of FEL2014* (JACoW, CERN, Geneva, 2014), p. 649.

[10] S. Casalbuoni, A. Cecilia, S. Gerstl, N. Glamann, A. W. Grau, T. Holubek, C. Meuter, D. Saez de Jauregui, R. Voutta, C. Boffo, Th. Gerhard, M. Turenne, and W. Walter, Characterization and long term operation of a novel superconducting undulator with 15 mm period length in a synchrotron light source, Phys. Rev. ST Accel. Beams **19**, 110702 (2016).

[11] Y. Ivanyushenkov, K. Harkay, M. Borland, R. Dejus, J. Dooling, C. Doose, L. Emery, J. Fuerst, J. Gagliano, Q. Hasse, M. Kasa *et al.*, Development and operating experience of a short-period superconducting undulator at the Advanced Photon Source, Phys. Rev. ST Accel. Beams **18**, 040703 (2015).

[12] E. Trakhtenberg, Y. Ivanyushenkov, C. Doose, and M. Kasa, Design of the magnet structure for the APS superconducting undulator, in *Proceedings of MEDSI 2010* (Diamond Light Source Ltd., Didcot, 2010).

[13] J. Fuerst, C. Doose, Q. Hasse, Y. Ivanyushenkov, M. Kasa, E. Moog, J. Pfotenhauer, D. Potratz, D. Skiadopoulos, V. Syrovatin, and E. Trakhtenberg, Cryostat design and development for a superconducting undulator for the APS, AIP Conf. Proc. **1434**, 901 (2012).

[14] D. Potratz, J. Pfotenhauer, Q. Hasse, Y. Ivanyushenkov, E. Moog, and R. Kustom, A helium thermosiphon cooling loop for the APS superconducting undulator, AIP Conf. Proc. **1434**, 1991 (2012).

[15] R. Merl and G. Decker, Design of the digitizing beam position limit detector, in *Beam Instrumentation Workshop*, AIP Proc. No. 451 (AIP, New York, 1999), p. 575.

[16] R. Voutta, S. Gerstl, S. Casalbuoni, A. W. Grau, T. Holubek, D. Saez de Jauregui, R. Bartolini, M. P. Cox, E. C. Longhi, G. Rehm, J. C. Schouten, R. P. Walker, M. Migliorati, and B. Spataro, Cold vacuum chamber for diagnostics: Analysis of the measurements at the Diamond Light Source and impedance bench measurements, Phys. Rev. ST Accel. Beams **19**, 053201 (2016).

[17] O. Chubar, P. Elleaume, and J. Chavanne, Computing 3D magnetic fields from insertion devices, in *Proceedings of the Particle Accelerator Conference, Vancouver, BC, Canada, 1997* (IEEE, New York, 1997), p. 3509.

[18] OPERA FEA Simulation Software, http://operafea.com.

[19] C. Doose and M. Kasa, Magnetic measurements of the first superconducting undulator at the Advanced Photon Source, in *Proceedings of the 25th Particle Accelerator Conference, PAC-2013, Pasadena, CA, 2013* (IEEE, New York, 2013), THPBA06, p. 1238.

[20] K. C. Harkay, L. Boon, M. Borland, L. Emery, R. L. Kustom, V. Sajaev, Y. Shiroyanagi, and A. Xiao, Beam-based alignment of the first superconducting undulator at the APS, in *Proceedings of the 2013 North American Particle Accelerator Conference NA-PAC'13, Pasadena, California, 2013* (JACoW, CERN, Geneva, 2013), WEPSM07.

[21] J. M. Penicka, C. Doose, K. Harkay, Q. Hasse, W. Jansma, Y. Ivanyushenkov, M. Kasa, D. Skiadopoulos, E. M. Trakhtenberg, and S. Wesling, Alignment of superconducting undulators at the APS, in *Proceedings of the 13th International Workshop on Accelerator Alignment (IWAA2014), Beijing, China, 2014* (Integrated Digital Conference, 2014).

[22] Y. Iwamoto, N. Kimura, T. Ogitsu, H. Ohhata, T. Nakamoto, K. Tanabe, A. Ichikawa, and A. Yamamoto, Quench stability against beam-loss in superconducting magnets at the 50 GeV proton beam line for the J-PARC neutrino experiment, IEEE Trans. Appl. Supercond. **14**, 592 (2004).

[23] J. C. Schouten and E. C. M. Rial, Electron beam heating and operation of the cryogenic undulator and superconducting wiggler at Diamond, in *Proceedings of the 2nd International Particle Accelerator Conference, San Sebastián, Spain* (EPS-AG, Spain, 2011), p. 3323.

[24] D. Robin *et al.*, Superbend upgrade on the Advanced Light Source, Nucl. Instrum. Methods Phys. Res., Sect. A **538**, 65 (2005).

[25] W. A. Wurtz *et al.*, Preventing superconducting wiggler quench during beam loss at the Canadian Light Source, in *Proceedings of the 5th International Particle Accelerator Conference IPAC2014, Dresden, Germany, 2014* (JACoW, CERN, Geneva, 2014), p. 1992.

[26] K. C. Harkay, J. C. Dooling, Y. Ivanyushenkov, R. Laird, F. K. Lenkszus, C. C. Putnam, V. Sajaev, and J. Wang, Development of an abort kicker at APS to mitigate beam loss-induced quenches of the superconducting undulator, in *Proceedings of the 6th International Particle Accelerator Conference IPAC2015, Richmond, VA, USA, 2015* (JACoW, CERN, Geneva, 2015), p. 1787.

[27] K. C. Harkay, J. C. Dooling, V. Sajaev, and J. Wang, Operational experience with beam abort system for superconducting undulator quench mitigation, in Proceedings of the 2016 North American Particle Accelerator Conference NAPAC2016, Chicago, USA, 2016, WEPOB05 (JACoW, CERN, Geneva, 2016), p. 890.

[28] J. Carwardine and F. Lenkszus, Real-time orbit feedback at the APS, in *BIW98*, AIP Conf. Proc. No. 451 (AIP, New York, 1998), pp. 125–144.

[29] S. D. Shastri, K. Fezzaa, A. Mashayekhi, W.-K. Lee, P. B. Fernandez, and P. L. Lee, Cryogenically cooled, bent double-Laue monochromator for high-energy undulator x-rays (50–200 keV), J. Synchrotron Radiat. **9**, 317 (2002).

[30] T. Tanaka and H. Kitamura, SPECTRA: A synchrotron radiation calculation code, J. Synchrotron Radiat. **8**, 1221 (2001).